Journal of Alloys and Compounds 793 (2019) 599–603

Contents lists available at ScienceDirect

Journal of Alloys and Compounds

journal homepage: http://www.elsevier.com/locate/jalcom

Modified band alignment at multilayer MoS_2/Al_2O_3 heterojunctions by nitridation treatment

Xinke Liu [a], Kuilong Li [b, *], Xiaojuan Sun [a], Zhiming Shi [a], Zhonghui Huang [c], Zhiwen Li [c], Long Min [c], Venkatadivakar Botcha [c], Xingyuan Chen [d], Xiangfu Xu [d], Dabing Li [a, e, **]

[a] State Key Laboratory of Luminescence and Applications, Changchun Institute of Optics, Fine Mechanics and Physics, Chinese Academy of Sciences, Changchun 130033, China
[b] School of Electronic and Information Engineering (Department of Physics), Qilu University of Technology (Shandong Academy of Sciences), Jinan, 250353, China
[c] College of Materials Science and Engineering, Shenzhen University, 3688 Nanhai Ave, Shenzhen, 518060, China
[d] Department of Physics, School of Science, Guangdong University of Petrochemical Technology, Maoming, Guangdong 525000, China
[e] Center of Materials Science and Optoelectronics Engineering, University of Chinese Academy of Sciences, Beijing 100049, China

ARTICLE INFO

Article history:
Received 20 February 2019
Received in revised form
19 April 2019
Accepted 22 April 2019
Available online 24 April 2019

Keywords:
Multilayer MoS_2
Al_2O_3 surface
NH_3 treatment
Band alignment

ABSTRACT

Interface engineering plays a decisive role in the two-dimensional material/high-κ oxide heterojunction-based devices. In this work, the effects of NH_3 plasma interface treatment on the energy band alignment at multilayer MoS_2/Al_2O_3 heterostructures were explored using x-ray photoelectron spectroscopy. A type-I band alignment was formed with valence band offset (VBO) and conduction band offset (CBO) about 3.67 eV and 2.33 eV, respectively. Significantly, the CBO was enlarged by about 0.45 eV after the plasma treatment, which was mainly attributed to the increased separation between the Al 2p core-level energy and valence band maximum. This interesting finding provides a significant guidance for the band adjustment at the interface and further applications of multilayer MoS_2 in electronic devices.

1. Introduction

In modern semiconductor-based devices such as lasers, light emitting diodes, photodetectors, transistors and so on, heterojunctions (HJs) play a key role owing to that their electrical and optical properties are mainly controlled by the band alignment at the HJs. However, the lattice mismatch and interfacial defects at the interfaces severely limit the development of HJ devices based on conventional bulk semiconductors. Fortunately, since the discovery of graphene in 2004 [1], atomically thin two dimensional (2D) materials have opened a new door for the development of semiconductor devices due to their unique structures, electronic, optical, mechanical, and thermal properties [2–4]. Especially, the formation of van der Waals bonded heterostructures between 2D layers potentially permit to create any desirable HJs [5–7]. Among the 2D semiconductors, MoS_2 as a typical representative has drawn an increasing attention due to its wide applications in optoelectronic and nanoelectronic technologies [8–11]. Monolayer MoS_2 contains a hexagonal trilayer with one Mo layer sandwiched between two sulfur layers, and the neighboring MoS_2 layers were weakly attached by van der Waals forces. Meanwhile, the band gap of MoS_2 was strongly related to the layer number, with a direct bandgap of about 1.80 eV for monolayer and indirect bandgap of 1.20 eV for bulk layers. Although multilayer MoS_2 have been seriously restricted in the application of photonic devices by the indirect bandgap, it has already been shown to enable the channel of metal-insulator-semiconductor transistors scaled down profoundly [12–14]. Furthermore, multilayer MoS_2 can facilitate transistors with very steep sub-threshold slope and high drive current which is attribute to the high density of states [15,16].

Currently, multilayer MoS_2/wide bandgap insulator HJs have been an indispensable part in the MoS_2-based electronic devices such as high frequency integrated logic circuits and nonvolatile memory. SiO_2 as the typical and most common used oxide insulator has been unable to satisfy the requirement of enhanced specific capacitance, low gate leakage current, and high carrier mobility in

* Corresponding author.
** Corresponding author. Center of Materials Science and Optoelectronics Engineering, University of Chinese Academy of Sciences, Beijing 100049, China.
E-mail addresses: likuilong123@126.com (K. Li), lidb@ciomp.ac.cn (D. Li).

https://doi.org/10.1016/j.jallcom.2019.04.227
0925-8388/

the related devices. High-κ oxides (e.g. Al_2O_3) were proved to improve the carrier mobility significantly owing to the dielectric screening effects [17,18]. Therefore, high-κ oxides have great potential applications in multilayer-based MoS_2 transistors. In addition, it is essential to point out that the characteristics of the MoS_2-based electronic devices are critically sensitive to the band alignment at the MoS_2/oxide HJ interface which strongly affect electron and hole transport property in the form of conduction band offset (CBO) and valence band offset (VBO). The VBO and CBO should be sufficiently large enough to reduce the injection of holes and electrons [19], respectively. Meanwhile, the defects and charges located at the semiconductor/oxide HJ interface also exert great influences on the energy band profile and need to be optimized using passivation technology. For Al_2O_3 oxide, NH_3 treatment on the surface has already been proved to be an effective surface engineering method to reduce the surface or interface defects [20]. In this paper, we investigated the band alignment at multilayer MoS_2/Al_2O_3 HJs, and the effects of NH_3 treatment on the band offset at MoS_2/Al_2O_3 interface was explored by x-ray photoelectron spectroscopy (XPS) measurements, which provides a significant guidance for the band adjustment at the interface and further applications of MoS_2 in electronic devices.

2. Experiments

The multilayer MoS_2/Al_2O_3 samples investigated in this paper were prepared by the PMMA method. Firstly, large area, continuous multilayer MoS_2 films were grown on SiO_2/Si substrates using chemical vapor deposition method as shown in Fig. 1(a). During the growing process, MoO_3 and sulfur powder were employed as the Mo and S sources with Ar as the carrier gas, respectively. Meanwhile, the growth temperature was located at 800 °C, and the growth time was about 5 min. Then, the Al_2O_3 dielectric oxide on Si was grown by atomic layer deposition system at 200 °C, using trimethylaluminium and H_2O as precursors, and the thickness was about 8.0 nm. The nitridation process on Al_2O_3 surface was carried out by employing low-energy NH_3 plasma treatments. By optimizing the conditions of plasma treatment in order to reduce the defect density at the interface, the RF power and flow rate were fixed at 200 W and 150 sccm, respectively. Meanwhile, the plasma treatment time was about 120 s and the pressure was kept at 100 Pa during the process. Then obvious N 1s peak located at about 398.74 eV was observed in the XPS spectrum shown in Fig. 1(b). For the reference sample, no NH_3 plasma treatment was implemented on Al_2O_3 surface. Lastly, the multilayer MoS_2 film were transferred onto the prepared Al_2O_3/Si substrates. Raman spectra at room temperature were collected through a Raman spectrophotometer system (Horiba Scientific, Labram HR evolution). The XPS measurements were performed using a VG ESCALAB 220i-XL system with a monochromatic Al Ka source at the power of 150 W. The photon energy of the x-ray source is about 1486.6 eV. During the measurements, XPS spectra were acquired using 20 eV pass energy, and a charge neutralizer was used to prevent charging. The XPS binding energy was calibrated using pure gold, silver, and copper standard samples by setting the Au 4f7/2, Ag 3d5/2, and Cu 2p3/2 peaks at 83.986 ± 0.02 eV, 368.266 ± 0.02 eV, and 932.676 ± 0.02 eV, respectively. The Fermi level edge was calibrated using pure nickel (Ni) and setting the binding energy at 0.00 ± 0.02 eV. In addition, C 1s peak (284.8 eV) was used to correct the core-level binding energy in order to eliminate the sample surface differential charging effect.

3. Results and discussions

Raman spectroscopy as a powerful tool to investigate the optical quality and to ascertain the layer number of 2D materials was performed for the samples. Fig. 1(c) shows the Raman spectrum of the multilayer MoS_2 which were grown on SiO_2/Si substrate and transferred onto Al_2O_3 oxide. Obviously, two typical Raman modes, E^1_{2g} (382.70 cm^{-1}) and A_{1g} (408.05 cm^{-1}) were observed, and the difference between them is 25.35 cm^{-1}, indicating the film layers was more than five [21]. Furthermore, the cross-sectional transmission electron microscopy (TEM) result displayed in the inset of Fig. 1(c) confirmed this inference as shown that the thickness is about 3.93 nm, corresponding to six layers. Meanwhile, the Raman position and full width at the half maximum of the peaks almost kept the same before and after transfer, demonstrating the optimized transfer process largely retained the material quality.

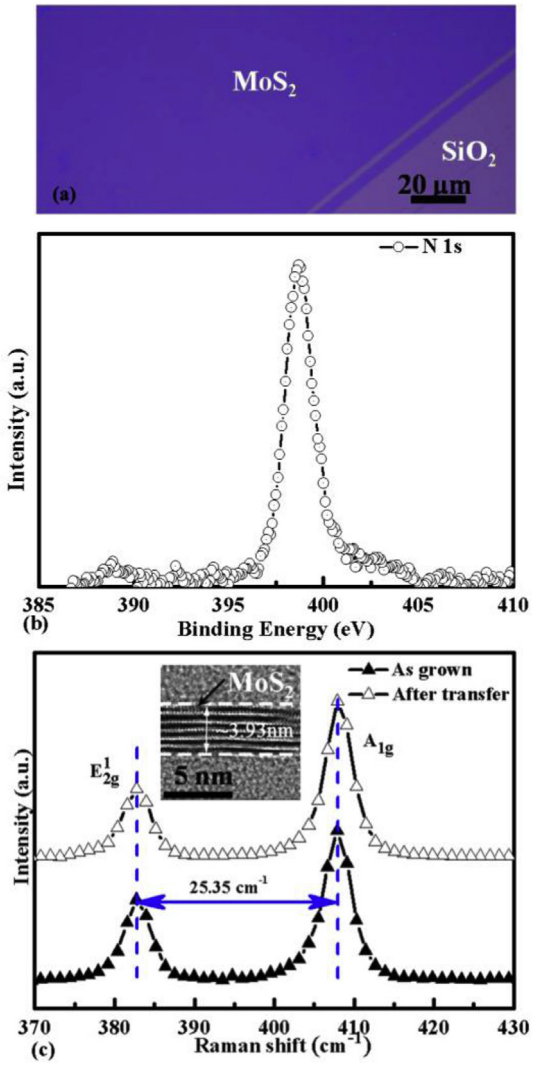

Fig. 1. (a) The optical micrograph of large area multilayer MoS_2 grown on SiO_2/Si substrate; (b) the N 1s XPS spectrum of the Al_2O_3 with NH_3 plasma treatment; (c) The Raman spectroscopy of the multilayer MoS_2 film before and after transfer. The inset is the cross-sectional TEM image of the MoS_2, which identified the layers of MoS_2.

XPS has been extensively employed to investigate the energy band offset at MoS_2-based HJs, such as MoS_2/GaN [22], MoS_2/$In_{0.15}Al_{0.85}N$ [23], MoS_2/SiO_2 [24], MoS_2/HfO_2 [25] and so on. The energy core level and valence band spectra of MoS_2 and Al_2O_3 were shown in Fig. 2. The VBO ΔE_v can be calculated according the following formula [26].

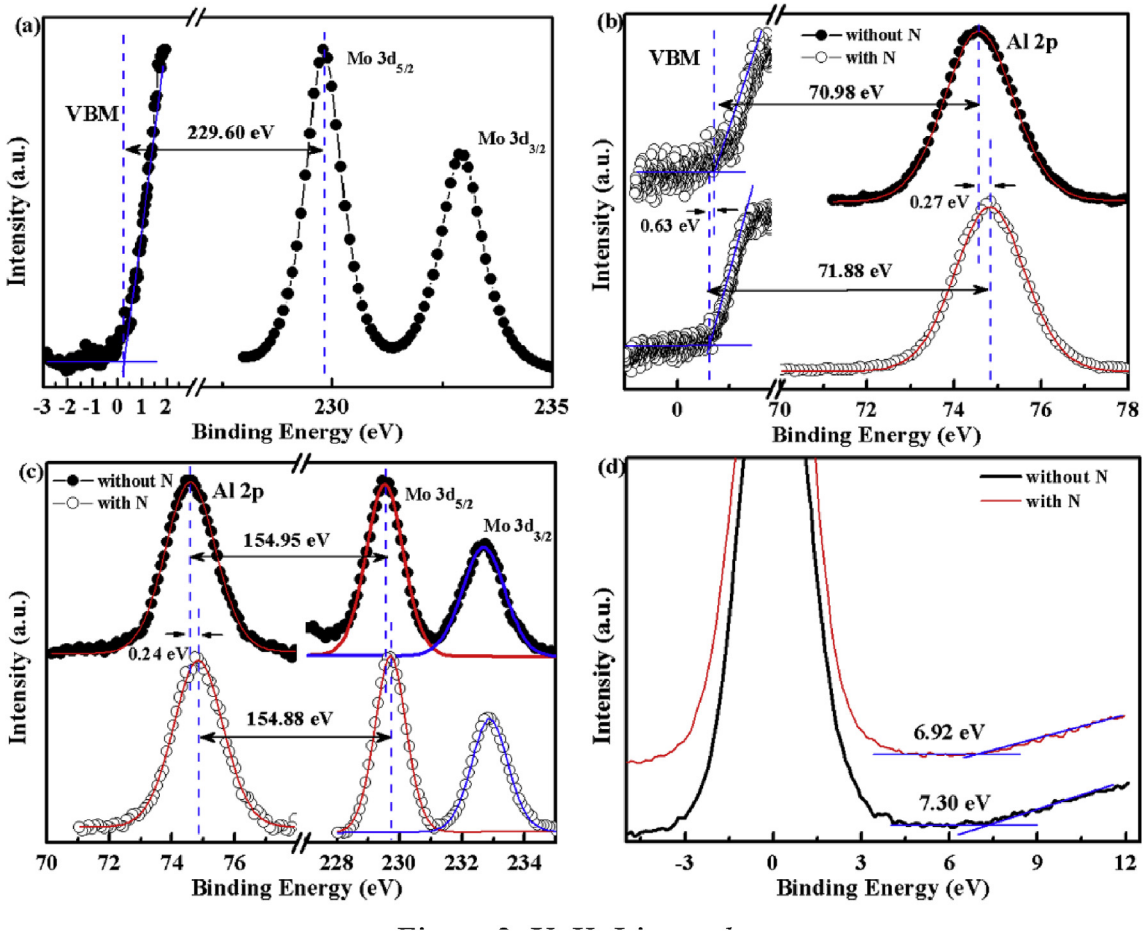

Fig. 2. The core-level and valence band spectra for (a) multilayer MoS_2 and (b) bare Al_2O_3 without and with NH_3 plasma treatment. (c) The corresponding Al 2p and Mo3d core-level energy spectrum collected from both multilayer MoS_2/Al_2O_3 samples. The VBM is obtained from the intercept of the slope at the leading edge of the valence band spectrum with the base line. (d) The O 1s photoelectron energy loss spectra for the Al_2O_3 oxide.

$$\Delta E_v = \left(E_{cl}^{MoS_2} - E_v^{MoS_2}\right) - \left(E_{cl}^{Al_2O_3} - E_v^{Al_2O_3}\right) - \left(E_{cl}^{H-MoS_2} - E_{cl}^{H-Al_2O_3}\right) \quad (1)$$

where $E_{cl}^{MoS_2}$ and $E_v^{MoS_2}$ represent the core-level and valence band maximum (VBM) energy value of MoS_2 obtained from multilayer MoS_2, respectively; $E_{cl}^{Al_2O_3}$ and $E_v^{Al_2O_3}$ are the related core-level and VBM energy of bare Al_2O_3, respectively; $E_{cl}^{H-MoS_2}$ and $E_{cl}^{H-Al_2O_3}$ correspond to the core-level energy of MoS_2 and Al_2O_3, respectively, which were derived from the multilayer MoS_2/Al_2O_3 HJs. Fig. 2(a) showed the Mo 3d core-level and valence band spectrum collected from multilayer MoS_2. Apparently, the Mo 3d core level was reconstituted with $3d_{5/2}$ (229.86 ± 0.05 eV) and $3d_{3/2}$ (232.94 ± 0.05 eV) two peaks, and the binding energy difference was about 3.08 eV induced by the spin-orbit splitting. The VBM with respect to the Fermi level energy (located at zero) was extrapolated from the intercept between the slope of the leading edge and the base line [27,28]. Then the energy separation between Mo $3d_{5/2}$ and VBM was 229.60 ± 0.05 eV. As a result, the first bracket term in Eq. (1) is about 229.60 eV just as labeled in Fig. 2(a). For the bare Al_2O_3 oxide without NH_3 treatment, the VBM was 3.59 ± 0.05 eV, while the surface nitridation made the VBM shifted towards Fermi level by 0.63 ± 0.05 eV as shown in Fig. 2(b), indicating this passivation technology exerted a significant influence on the valence band of Al_2O_3. Similarly, the core-level binding energy of Al 2p was shifted upwards 0.27 ± 0.05 eV after NH_3 treatment in comparison with that without nitridation. Then, the second bracket term in Eq. (1) was 70.98 ± 0.05 eV and 71.88 ± 0.05 eV for the multilayer MoS_2/Al_2O_3 samples without and with NH_3 plasma treatment, respectively. Furthermore, Fig. 2(c) showed the core-level binding energy separation between Al 2p and Mo $3d_{5/2}$ obtained from multilayer-MoS_2/Al_2O_3 HJs, 154.95 ± 0.05 eV for the sample without interface passivation while 154.88 ± 0.05 eV for the plasma treated sample, which corresponded to the third bracket term values in Eq. (1). Consequently, the ΔE_v between multilayer MoS_2 and Al_2O_3 was about 3.67 ± 0.05 eV and 2.84 ± 0.05 eV for the sample without and with NH_3 treatment, respectively. Subsequently, the CBO value ΔE_c was calculated based on the energy band gap of Al_2O_3 ($E_g^{Al_2O_3}$) and multilayer MoS_2 ($E_g^{MoS_2}$) expressed as

$$\Delta E_c = E_g^{Al_2O_3} - \Delta E_v - E_g^{MoS_2} \quad (2)$$

where the $E_g^{Al_2O_3}$ was obtained from the O1s loss energy spectrum as shown in Fig. 2(d). Obviously, $E_g^{Al_2O_3}$ for the Al_2O_3 without NH_3 treatment was about 7.30 ± 0.05 eV extrapolated from the separation between the core-level energy of Al—O bonds and the linear edge base line. In compare with this sample, interface nitridation reduced the energy band gap of Al_2O_3 by about 0.38 eV. While for multilayer MoS_2, the electronic band gap $E_g^{MoS_2}$ was set at 1.30 eV [29] in this work. As a result, the ΔE_c value for the samples without and with plasma treatment determined from Eq. (2) was

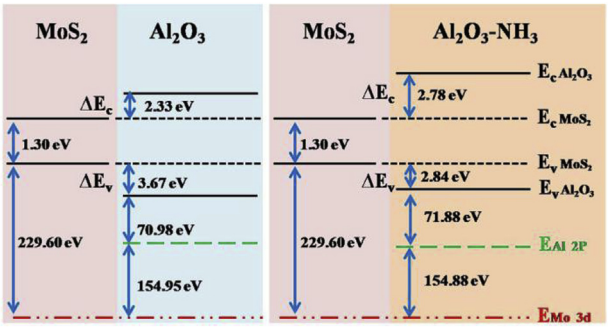

Fig. 3. The schematic structure of the energy band alignment at the multilayer-MoS_2/Al_2O_3 interface without and with NH_3 plasma treatment.

2.33 ± 0.05 eV and 2.78 ± 0.05 eV, respectively. Then, the experimental determined band alignment at MoS_2/Al_2O_3 HJs was illustrated by a schematic structure labeled with the parameters obtained from XPS results as shown in Fig. 3. It is meaningful to find out that on one hand, a type-I band alignment was formed at the HJ with both CBO and VBO larger than 1.0 eV; on the other hand, the NH_3 interface treatment enlarged the CBO value by about 0.45 eV, which is profoundly beneficial to the related n type MoS_2-based transistors. For MoS_2/Al_2O_3 heterojunctions, the band alignment has been investigated with valence band offset about 3.51 eV for multilayer MoS_2 [30], which is consistence with the obtained value here, whereas the difference in conduction band offset is mainly introduced by the variation of the bandgap of Al_2O_3. Recently, Zhang et al. have reported that the nitridation interfacial layer at MoS_2/GaN HJs introduced by the N_2 plasma treatment to GaN surface increased the CBO by about 0.5 eV, which was attributed to the upward shift of MoS_2 band edge [31]. For the CHF_3 treated MoS_2/HfO_2 HJs, the plasma has brought down the CBO value [25]. Herein, NH_3 treatment as a relatively mature passivation technology for nitrides or high-κ oxides evidently adjusted the band alignment at 2D/3D heterostructures, providing a promising way to the band modification.

The XPS experiments have demonstrated that NH_3 plasma treatment to Al_2O_3 surface significantly affect the valence band edge of Al_2O_3 and the core-level energy of Al 2p, indicating this passivation technology imposed a great effect on the electronic structures of Al_2O_3. Then a calculation was implemented using Vienna ab initio simulation package (VASP) code based on density functional theory (DFT) [32]. The Perdew-Burke-Ernzerhof version of the generalized gradient approximation (PBE-GGA) was selected for the exchange and correlation potential and the projector augmented wave potential (PAW) was employed to treat the ion-electron interactions [33,34]. We used $2 \times 2 \times 2$ supercells containing 144 Al atoms and 96 O atoms for calculations. The relaxed lattice constant for primitive cell are a = 4.759 Å and c = 12.991 Å, while for the supercell, the related value for a and c are 9.518 Å and 25.982 Å, respectively. The cutoff energy for the plane-wave basis expansion was set to be 450 eV, and a Monkhorst–Pack k-mesh of $3 \times 2 \times 1$ was used to the Brillouin zone integration in the structure optimization and total energy calculation [35]. All the atoms were relaxed to their equilibrium positions when the total energy changes during the optimization finally converged to less than 10^{-6} eV/atom, the force and stress on each atom in the crystal was converged to 0.003 eV/nm and 0.05 GPa, respectively. Meanwhile, the convergence criteria for the displacement was set to 1×10^{-4} nm. Fig. 4(a)-(f) show the band structures of Al_2O_3 without and with NH_3 treatment and the corresponding total density of state (DOS) and partial density of state (PDOS). Apparently, the formation of interfacial layer by the nitridation introduces mid-gap states at the energy gap and thereby reduces the bandgap as shown in Fig. 4(e). Then the strong interactions between Al and N atoms makes the Al-p energy level moving far away from the VBM just as demonstrated from the XPS results shown in Fig. 2(b) that the separation between Al 2p and VBM was enlarged by about 0.90 eV

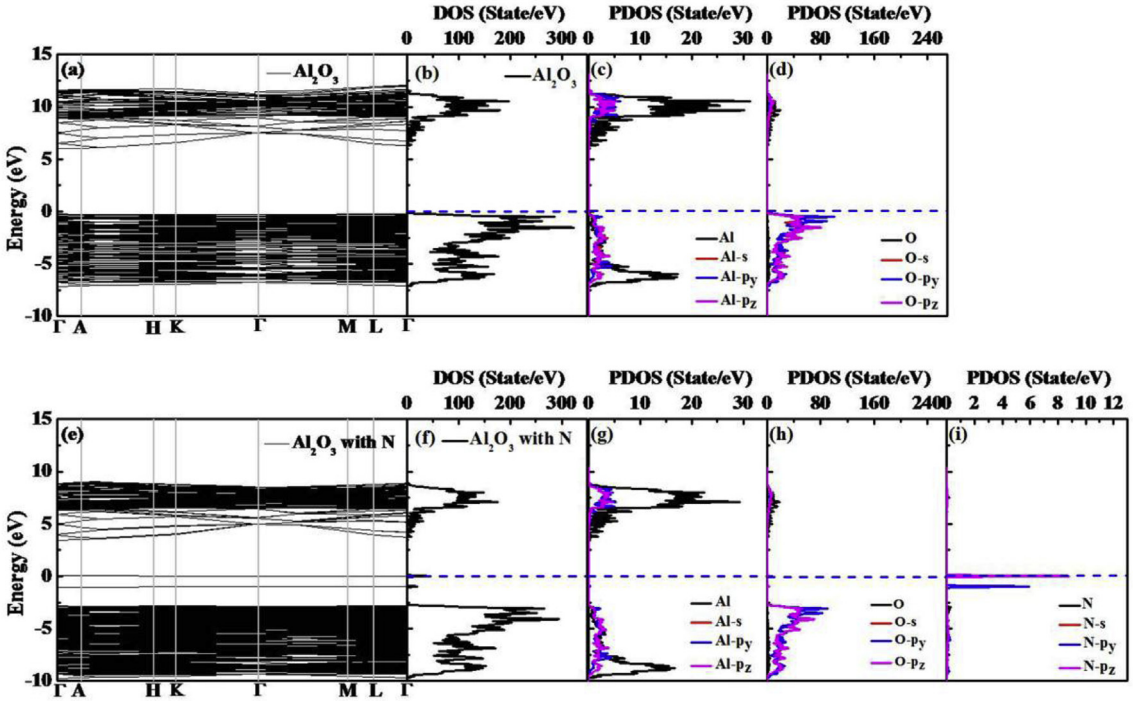

Fig. 4. The calculated energy band structure, total density of states (DOS), and partial density of states (PDOS) for the samples without NH_3 treatment (a)–(d) and with NH_3 treatment (e)–(i).

by nitridation in comparison with the sample without NH_3 treatment. Meanwhile, the interface mid-gap states may enhance the electron transfer between the MoS_2 and Al_2O_3, which contributes to the upshift of Mo 3d core-level energy. For MoS_2-based electronic devices, the mid-gap states may deteriorate the device performances acting as electron leakage channel. However, herein, for multilayer-MoS_2 FETs, the electrons were mainly transported in the top few layers due to the electrons were scattered away from the interface by the enhanced potential barrier of the conduction band offset. For monolayer-MoS_2/Al_2O_3 heterojunctions, this effect needs to be further investigated and optimized. Therefore, the NH_3 plasma treatment is beneficial to the multilayer MoS_2 based electronic devices.

4. Conclusions

In conclusion, the influences of NH_3 plasma treatment to Al_2O_3 surface on the band alignment of multilayer-MoS_2/Al_2O_3 heterostructures were explored experimentally and theoretically. The formation of the nitridation interfacial layer significantly enlarge the conduction band offset by about 0.45 eV, which was primarily attributed to the increased separation between the Al 2p core-level and valence band maximum. The surface passivation by NH_3 plasma treatment provides a promising way to modulate the energy band alignment at heterointerfaces, which exerts great impacts on the related devices.

Acknowledgement

This work is supported by National Key Research and Development Program of China (2017YFB0403000), and National Science Fund for Distinguished Young Scholars (61725403), the Special Fund for Research on National Major Research Instruments (61827813), the National Natural Science Foundation of China (61874118, 61804086), Natural Science Foundation of Shandong Province (ZR2017LF022), and CAS Pioneer Hundred Talents Program.

References

[1] K.S. Novoselov, A.K. Geim, S.V. Morozov, D. Jiang, Y. Zhang, S.V. Dubonos, I.V. Grigorieva, A.A. Firsov, Electric field effect in atomically thin carbon films, Science 306 (2004) 666–669.
[2] B. Radisavljevic, A. Radenovic, J. Brivio, V. Giacometti, A. Kis, Single-layer MoS_2 transistors, Nat. Nanotechnol. 6 (2011) 147.
[3] B.W.H. Baugher, H.O.H. Churchill, Y. Yang, P. Jarillo-Herrero, Optoelectronic devices based on electrically tunable p–n diodes in a monolayer dichalcogenide, Nat. Nanotechnol. 9 (2014) 262.
[4] J. Yang, Z. Wang, F. Wang, R. Xu, J. Tao, S. Zhang, Q. Qin, B. Luther-Davies, C. Jagadish, Z. Yu, Y. Lu, Atomically thin optical lenses and gratings, Light: Science & Applications 5 (2016) e16046.
[5] Y. Liu, N.O. Weiss, X. Duan, H.-C. Cheng, Y. Huang, X. Duan, Van der Waals heterostructures and devices, Nat. Rev. Mater. 1 (2016) 16042.
[6] H. Terrones, F. López-Urías, M. Terrones, Novel hetero-layered materials with tunable direct band gaps by sandwiching different metal disulfides and diselenides, Sci. Rep. UK 3 (2013) 1549.
[7] M. Chhowalla, D. Jena, H. Zhang, Two-dimensional semiconductors for transistors, Nat. Rev. Mater. 1 (2016) 16052.
[8] H. Wang, L. Yu, Y.-H. Lee, Y. Shi, A. Hsu, M.L. Chin, L.-J. Li, M. Dubey, J. Kong, T. Palacios, Integrated circuits based on bilayer MoS_2 transistors, Nano Lett. 12 (2012) 4674–4680.
[9] J. Pu, Y. Yomogida, K.-K. Liu, L.-J. Li, Y. Iwasa, T. Takenobu, Highly flexible MoS_2 thin-film transistors with ion gel dielectrics, Nano Lett. 12 (2012) 4013–4017.
[10] F.K. Perkins, A.L. Friedman, E. Cobas, P.M. Campbell, G.G. Jernigan, B.T. Jonker, Chemical vapor sensing with monolayer MoS_2, Nano Lett. 13 (2013) 668–673.
[11] Z. Yin, H. Li, H. Li, L. Jiang, Y. Shi, Y. Sun, G. Lu, Q. Zhang, X. Chen, H. Zhang, Single-layer MoS_2 phototransistors, ACS Nano 6 (2012) 74–80.
[12] R. Ganatra, Q. Zhang, Few-layer MoS_2: a promising layered semiconductor, ACS Nano 8 (2014) 4074–4099.
[13] A. Nourbakhsh, A. Zubair, S. Joglekar, M. Dresselhaus, T. Palacios, Subthreshold swing improvement in MoS_2 transistors by the negative-capacitance effect in a ferroelectric Al-doped-HfO_2/HfO_2 gate dielectric stack, Nanoscale 9 (2017) 6122–6127.
[14] A. Nourbakhsh, A. Zubair, R.N. Sajjad, K.G. avakkoli, W. Chen, S. Fang, X. Ling, J. Kong, M.S. Dresselhaus, E. Kaxiras, K.K. Berggren, D. Antoniadis, T. Palacios, MoS_2 field-effect transistor with sub-10 nm channel length, Nano Lett. 16 (2016) 7798–7806.
[15] D. Sarkar, X. Xie, W. Liu, W. Cao, J. Kang, Y. Gong, S. Kraemer, P.M. Ajayan, K. Banerjee, A subthermionic tunnel field-effect transistor with an atomically thin channel, Nature 526 (2015) 91.
[16] S. Kim, A. Konar, W.S. Hwang, J.H. Lee, J. Lee, J. Yang, C. Jung, H. Kim, J.B. Yoo, J.Y. Choi, Y.W. Jin, S.Y. Lee, D. Jena, W. Choi, K. Kim, High-mobility and low-power thin-film transistors based on multilayer MoS_2 crystals, Nat. Commun. 3 (2012) 1011.
[17] H. Liu, K. Xu, X. Zhang, P.D. Ye, The integration of high-k dielectric on two-dimensional crystals by atomic layer deposition, Appl. Phys. Lett. 100 (2012) 152115.
[18] M.R. Laskar, L. Ma, S. Kannappan, P.S. Park, S. Krishnamoorthy, D.N. Nath, W. Lu, Y. Wu, S. Rajan, Large area single crystal (0001) oriented MoS_2, Appl. Phys. Lett. 102 (2013) 252108.
[19] J. Tao, J.W. Chai, Z. Zhang, J.S. Pan, S.J. Wang, The energy-band alignment at molybdenum disulphide and high-k dielectrics interfaces, Appl. Phys. Lett. 104 (2014) 232110.
[20] Y.J. Cho, H. Cha, H.S. Chang, Plasma nitridation of atomic layer deposition (ALD) Al_2O_3 by NH_3 in plasma-enhanced chemical vapor deposition (PECVD) for silicon solar cell, Surf. Coating. Technol. 307 (2016) 1096–1099.
[21] C. Lee, H. Yan, L.E. Brus, T.F. Heinz, J. Hone, S. Ryu, Anomalous lattice vibrations of single- and few-layer MoS_2, ACS Nano 4 (2010) 2695–2700.
[22] M. Tangi, P. Mishra, T.K. Ng, M.N. Hedhili, B. Janjua, M.S. Alias, D.H. Anjum, C.-C. Tseng, Y. Shi, H.J. Joyce, L.-J. Li, B.S. Ooi, Determination of band offsets at GaN/single-layer MoS_2 heterojunction, Appl. Phys. Lett. 109 (2016), 032104.
[23] M. Tangi, P. Mishra, M.-Y. Li, M.K. Shakfa, D.H. Anjum, M.N. Hedhili, T.K. Ng, L.-J. Li, B.S. Ooi, Type-I band alignment at $MoS_2/In_{0.15}Al_{0.85}N$ lattice matched heterojunction and realization of MoS_2 quantum well, Appl. Phys. Lett. 111 (2017), 092104.
[24] V.V. Afanas'ev, D. Chiappe, C. Huyghebaert, I. Radu, S. De Gendt, M. Houssa, A. Stesmans, Band alignment at interfaces of few-monolayer MoS_2 with SiO_2 and HfO_2, Microelectron. Eng. 147 (2015) 294–297.
[25] X. Liu, J. He, Q. Liu, D. Tang, F. Jia, J. Wen, Y. Lu, W. Yu, D. Zhu, W. Liu, P. Cao, S. Han, J. Pan, Z. He, K.-W. Ang, Band alignment of HfO_2/multilayer MoS_2 interface determined by x-ray photoelectron spectroscopy: effect of CHF_3 treatment, Appl. Phys. Lett. 107 (2015) 101601.
[26] E.A. Kraut, R.W. Grant, J.R. Waldrop, S.P. Kowalczyk, Precise determination of the valence-band edge in X-ray photoemission spectra: application to measurement of semiconductor interface potentials, Phys. Rev. Lett. 44 (1980) 1620–1623.
[27] S.W. King, C. Ronning, R.F. Davis, M.C. Benjamin, R.J. Nemanich, Dependence of (0001) GaN/AlN valence band discontinuity on growth temperature and surface reconstruction, J. Appl. Phys. 84 (1998) 2086–2090.
[28] M. Tangi, J. Kuyyalil, S.M. Shivaprasad, Optical bandgap and near surface band bending in degenerate InN films grown by molecular beam epitaxy, J. Appl. Phys. 114 (2013) 153501.
[29] W. Choi, M.Y. Cho, A. Konar, J.H. Lee, G.-B. Cha, S.C. Hong, S. Kim, J. Kim, D. Jena, J. Joo, S. Kim, High-detectivity multilayer MoS2 phototransistors with spectral response from ultraviolet to infrared, Adv. Mater. 24 (2012) 5832–5836.
[30] S.K. Pradhan, B. Xiao, A.K. Pradhan, Energy band alignment of high-k oxide heterostructures at MoS_2/Al_2O_3 and MoS_2/ZrO_2 interfaces, J. Appl. Phys. 120 (2016) 125305.
[31] Z. Zhang, Q. Qian, B. Li, K.J. Chen, Interface engineering of monolayer MoS_2/GaN hybrid heterostructure: modified band Alignment for photocatalytic water splitting application by nitridation treatment, ACS Appl. Mater. Interfaces 10 (2018) 17419–17426.
[32] M.D. Segall, J.D.L. Philip, M.J. Probert, C.J. Pickard, P.J. Hasnip, S.J. Clark, M.C. Payne, First-principles simulation: ideas, illustrations and the CASTEP code, J. Phys. Condens. Matter 14 (2002) 2717.
[33] J.P. Perdew, K. Burke, M. Ernzerhof, Generalized gradient approximation made simple, Phys. Rev. Lett. 77 (1996) 3865–3868.
[34] P.E. Blöchl, Projector augmented-wave method, Phys. Rev. B 50 (1994) 17953–17979.
[35] H.J. Monkhorst, J.D. Pack, Special points for Brillouin-zone integrations, Phys. Rev. B 13 (1976) 5188–5192.